






RESEARCH ARTICLE

Tracking the binding of multi-functional fluorescent tags for Alzheimer's disease using quantitative multiphoton microscopy

Rishyashring R. Iyer^{1,2}  | Carlos A. Renteria^{1,3}  | Lingxiao Yang^{1,2}  |
Janet E. Sorrells^{1,3}  | Jaena Park^{1,3} | Liang Sun⁴ | Zhengxin Yu⁴ |
Yiran Huang⁴ | Marina Marjanovic^{1,3,5} | Liviu M. Mirica^{1,4,5,6} |
Stephen A. Boppart^{1,2,3,5,7,8*} 

¹Beckman Institute for Advanced Science and Technology, University of Illinois at Urbana-Champaign, Urbana, Illinois, USA

²Department of Electrical and Computer Engineering, University of Illinois at Urbana-Champaign, Urbana, Illinois, USA

³Department of Bioengineering, University of Illinois at Urbana-Champaign, Urbana, Illinois, USA

⁴Department of Chemistry, University of Illinois at Urbana-Champaign, Urbana, Illinois, USA

⁵The Neuroscience Program, University of Illinois at Urbana-Champaign, Urbana, Illinois, USA

⁶Hope Center for Neurological Disorders, Washington University School of Medicine, St. Louis, Missouri, USA

⁷Carle Illinois College of Medicine, University of Illinois at Urbana-Champaign, Urbana, Illinois, USA

⁸Cancer Center at Illinois, University of Illinois at Urbana-Champaign, Urbana, Illinois, USA

*Correspondence

Stephen A. Boppart, University of Illinois at Urbana-Champaign, Urbana, Illinois, 61801, USA.

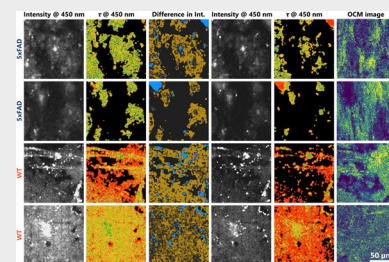
Email: boppart@illinois.edu

Funding information

Air Force Office of Scientific Research, Grant/Award Number: FA9550-17-1-0387; Graduate College, University of Illinois at Urbana-Champaign, Grant/Award Number: Mavis Future Faculty Fellowship; National Cancer Institute, Grant/Award Number: R01-CA241618; National Institute of Biomedical Imaging and Bioengineering, Grant/Award Number: T32-EB019944; National Institute of Environmental Health Sciences, Grant/Award Number: T32-ES007326; National Institute of General Medical Sciences, Grant/Award Number: R01-GM114588; National Science Foundation, Grant/Award Number: DGE-1746047

Abstract

A recent theranostic approach to address Alzheimer's disease (AD) utilizes multifunctional targets that both tag and negate the toxicity of AD biomarkers. These compounds, which emit fluorescence with both an activation and a spectral shift in the presence of A β , were previously characterized with traditional fluorescence imaging for binary characterization. However, these multifunctional compounds have broad and dynamic emission spectra that are dependent on factors such as the local environment, presence of A β deposits, etc. Since quantitative multiphoton microscopy is sensitive to the binding dynamics of molecules, we characterized the performance of two such compounds, LS-4 and ZY-12-OMe, using Simultaneous Label-free Autofluorescence Multi-harmonic (SLAM) microscopy and Fast Optical Coherence, Autofluorescence Lifetime imaging and Second harmonic generation (FOCALs) microscopy. This study shows that the combination of quantitative multiphoton imaging with multifunctional tags for



This is an open access article under the terms of the [Creative Commons Attribution-NonCommercial-NoDerivs](https://creativecommons.org/licenses/by-nc-nd/4.0/) License, which permits use and distribution in any medium, provided the original work is properly cited, the use is non-commercial and no modifications or adaptations are made.

© 2022 The Authors. *Journal of Biophotonics* published by Wiley-VCH GmbH.

AD offers new insights into the interaction of these tags with AD biomarkers and the theranostic mechanisms.

KEYWORDS

Alzheimer's disease, multimodal imaging, multiphoton microscopy, optical imaging, theranostics

1 | INTRODUCTION

Despite being the most common cause for dementia worldwide, the molecular complexity of Alzheimer's disease (AD) is poorly understood [1, 2]. As a pervasive neurodegenerative disorder, AD progresses slowly over decades with a disease progression that is characterized by the presence of amyloid-beta ($A\beta$) plaques in the brain and other parts of the central nervous system. $A\beta$ oligomers start appearing in the early stages of the disease; some forms of $A\beta$ oligomers are neurotoxic and the cause for neuronal degeneration [3, 4]. Therefore, $A\beta$ oligomers and plaque deposits may serve as both biomarkers for diagnostic purposes as well as for targets for therapeutic agents. Several small molecules with high affinity for $A\beta$ oligomers can permeate the blood–brain barrier, and these have been developed as potential theranostic agents for AD [5–8].

The Mirica group at the University of Illinois at Urbana-Champaign has developed several bi- and multifunctional small molecules that tag and inhibit the formation of $A\beta$ oligomers [9–11]. Essentially, these molecules contain a hydrophobic $A\beta$ -binding fragment and a hydrophilic metal-chelating azamacrocyclic that has been shown to counteract Cu^{2+} - $A\beta$ toxicity and rescue degenerating neurons in vitro. Copper (Cu) plays a role in the modulation of $A\beta$ aggregation and Cu^{2+} - $A\beta$ complex catalyzes the production of reactive oxygen species, which cause oxidative stress and neurotoxicity. Metal-chelating compounds remove Cu^{2+} from $A\beta$ aggregates and stop oxidative damage and subsequent cell death [12]. In this article, we investigate two of those compounds: LS-4 [9] and ZY-12-OMe [11] (Figure S1).

The $A\beta$ -binding hydrophobic fragment of LS-4 is a distyrylbenzene derivative, DF-9, that has a high affinity for $A\beta$ [13] and resembles the FDA-approved PET imaging agent, [^{18}F]florbetaben [14], which is a widely used amyloid dye [15]. The hydrophilic azamacrocyclic, 2,4-dimethyl-1,4,7-triazacyclononane (Me_2HTACN), has metal-chelating properties to counteract Cu^{2+} -induced neurotoxicity. Moreover, the 2-methoxy-phenol of the hydrophobic fragment resembles *o*-vanillin that has been shown to inhibit the formation of $A\beta$ oligomers [16]. LS-4 showed a 20- to 50-fold increase in fluorescence with 380

nm single-photon excitation in the presence of $A\beta$ fibrils and oligomers and showed blue-shifted emission spectra under different binding conditions. Additionally, it can penetrate the blood–brain barrier in vivo, and reduces the number of amyloid plaques and microglial activation in mouse models for AD (5x*FAD*) [9]. Two-month-old 5x*FAD* mice start exhibiting amyloid deposition and progressive neuronal loss that is characteristic for human AD. LS-4 was also shown to be fast-acting, binding to the $A\beta$ peptides within the first few hours. ZY-12-OMe contains a Me_2TACN with a methoxy group attached that is bound to a stilbene derivative. The fluorescence emission spectra of ZY-12-OMe shifts drastically from 550 to 480 nm in the presence of $A\beta$ aggregates, oligomers and fibrils due to the restriction in the rotation of the aromatic rings. Like LS-4, ZY-12-OMe could also penetrate the blood–brain barrier. Both compounds showed high correlation to dyes tagged with antibodies for $A\beta$ plaques [11]. Both ZY-12-OMe and LS-4 were shown to have very high binding affinity to different forms of $A\beta$ aggregates with dissociation constants >320 and 50 nM, respectively [9–11].

In this study, we evaluated the binding dynamics of LS-4 and ZY-12-OMe with quantitative multiphoton microscopy, tracking the changes to the fluorescence spectra, intensity, and lifetime. Compared with confocal microscopy, which has been previously used to track these small molecules in the brain, multiphoton microscopy has better spatial resolution, penetration depth and lower photobleaching that enable imaging the fast dynamics of these compounds over long durations. Multiphoton microscopy has enabled high-throughput studies of AD biomarkers for other common exogenous labels [17, 18]. We have previously described the simultaneous label-free autofluorescence multi-harmonic (SLAM) microscopy [19–21] and the fast optical coherence, autofluorescence lifetime imaging, and second harmonic generation (FOALS) microscopy [22] setups for label-free characterization of live in vitro, ex vivo, and in vivo samples.

SLAM microscopy causes simultaneous two-photon and three-photon excitation of fluorophores and harmonophores, and the emitted non-linear signals are measured in four spectral bands between 365–375, 420–

480, 540–570 and 580–640 nm to capture third-harmonic generation (THG), three-photon excitation fluorescence (3PEF), second harmonic generation (SHG), and two-photon excitation fluorescence (2PEF), respectively, at approximately 0.5 frames per second for a 200×200 pixel image. Label-free imaging using SLAM microscopy predominantly involves imaging of NAD(P)H using 3PEF, FAD using 2PEF, collagen using SHG, and optical heterogeneity using THG, and has primarily been directed for cancer imaging in prior studies [20, 21, 23]. The emission spectra of both LS-4 and ZY-12-OMe span 440 to 600 nm in the presence and absence of A β aggregates; they are expected to generate signals in the three latter detectors of SLAM microscopy, depending on their mode of interaction with the A β aggregates. Multispectral multiphoton microscopy enables a more comprehensive evaluation of the binding of the compounds within the first hour over an entire coronal slice of murine brain.

The restriction in the rotation of the aromatic rings of the two tested compounds upon binding to A β aggregates is not only expected to create a “turn-on” or activation effect and a shift in the emission spectrum, but also a change in the fluorescence lifetime due to a change in the molecular energy levels. FOCALS microscopy was designed to capture the 2PEF lifetime using fast fluorescence lifetime imaging microscopy (FLIM), along with optical coherence microscopy (OCM) for structural imaging. The multimodal images generated from FOCALS microscopy have been utilized to profile cells and tissues label-free under different imaging conditions. FLIM is more sensitive to the changes in fluorescence dynamics than intensity imaging alone. Fast FLIM can image several fields of view within the first few minutes of the compounds' interaction with the sample. Through GPU-accelerated processing and computational photon counting, fast FLIM in FOCALS microscopy utilizes the emitted photons more effectively than traditional FLIM techniques, is more accurate than comparable direct pulse-sampling-based fast FLIM techniques, and generates images in real-time [22, 24, 25]. Compared with wide field or confocal fluorescence imaging, techniques such as SLAM and FOCALS microscopy are multimodal, generate quantitative metrics, and are more sensitive to subtle molecular and environmental changes.

Using the 5xFAD model, the binding of LS-4 and ZY-12-OMe to A β deposits was evaluated following topical application on frozen brain slices and in fresh slices after intravenous injections. The binding of the compounds in brain slices within the first hour upon topical application was tracked in four spectral bands. Their performance corresponds to previously observed spectral characteristics. Additionally, compared with multispectral fluorescence imaging, FLIM characterized different binding

characteristics within a single spectral band. This was observed both in frozen slices for topical application within the first 5 to 30 min and in fresh brain slices following intravenous injections.

2 | METHODS

2.1 | Optical setups, image acquisition and processing

SLAM microscopy is sourced by supercontinuum generated from a photonic crystal fiber pumped by a 1030 nm fiber laser (Satsuma, Amplitude Systemes) and operating at a 20 MHz repetition rate with approximately 3.34 W of output power. A portion of this supercontinuum, ranging 1110 ± 30 nm, was shaped by an SLM-based pulse shaper (Biophotonics Solutions) to generate ultrafast pulses. The emitted fluorescence was collected using four photon-counting photomultiplier tubes (PMTs, H7421-40, Hamamatsu Corporation), simultaneously, between 365–375, 420–480, 540–570 and 580–640 nm. Data was acquired using a custom LabVIEW program with a mosaic functionality that enabled the acquisition of images from an entire transverse plane across a coronal murine brain slice ($\sim 6.4 \times 6.4$ mm²). The setup for SLAM microscopy has been previously described in detail by You et al [21]. The images for the pure compounds in phosphate buffered saline (PBS) were randomly sampled at multiple locations 5 to 10 μ m into the sample. The images of the brain slices were acquired as 200×200 pixel tiles spanning 400×400 μ m². A collection of 15–17 tiles in each direction were acquired to obtain one mosaic spanning the entire region of the brain slice.

The system setup for FOCALS microscopy has been previously described in detail by Iyer et al [22]. In brief, FOCALS microscopy obtains fast FLIM, OCM and SHG microscopy images simultaneously at 0.5 frames per second for 256×256 -pixel images. FOCALS microscopy is sourced by a tunable titanium-sapphire laser operating at 750 nm (MaiTai HP, Spectra Physics) and generating pulses <300 fs. The emitted spectrum was collected using an analog PMT (H10721-210, Hamamatsu Corporation), conditioned with a 1.5 GHz transimpedance amplifier (C5594, Hamamatsu Corporation) and sampled with a high-speed digitizer at 3.2 GS/s (ATS9373, AlazarTech) across 415 to 485 nm (or 468–552 nm, where specified). A part of the laser output was used to pump a photonic crystal fiber (LMA-PM-5, NKT Photonics) to obtain a broader spectrum that was then used to collect the OCM images in the spectral-domain using a fiber-based spectrometer (Cobra 800, Wasatch Photonics & spl4096-140km, Basler AG). The SHG signal for the 750 nm light

was minimal and therefore neglected in this study. Both setups used a 1.05-NA 25x water-immersion objective lens for this study (XLPLN25XWMP2, Olympus Corporation).

All steps to process the images and generate the figures in this article were done using MATLAB. The individual frames of the SLAM images within a mosaic were normalized with a 25-pixel 2D Gaussian filter applied across all frames in the 2PEF channel to remove vignette artifacts; the mosaics were assembled and normalized computationally. For analyzing the uptake of LS-4 or ZY-12-OMe, an intensity threshold of 20 was empirically determined after using a 5×5 2D Gaussian filter over the 2PEF channel to window the regions inside the brain from the background. The tiles at the edges with abnormal uptake, estimated as the tiles where over 25% of the pixels had non-zero intensities in the 3PEF channels, were excluded from the analysis. The four channels were normalized to the 90th percentile in each mosaic to enable them to fit on the same plot. All *p* values were calculated using two-way Student's *t* tests.

The FLIM data were processed in real-time on a GPU using our previously described algorithm for computational photon counting called Single-photon PEak Event Detection (SPEED) [24, 25] with 3×3 binning to gather enough photons for accurate 2PEF lifetime estimation (threshold was set to be 100 cumulative photons after binning) using phasor analysis. The OCM images are shown as the average projection of 6 en face planes around the focus (spanning 15 μm axially) and the color scale was set to span the 10th to 90th percentiles of intensity in the frame. For quantifying the spectral shift in fresh brain slices between the two spectral band, a subtractive metric was chosen over a ratiometric one to avoid the abnormal effects of a vanishing denominator.

2.2 | Materials and sample preparation

The procedures for the synthesis, characterization and validation of LS-4 and ZY-12-OMe were described previously [9, 11]. The synthesized compounds, at a concentration of 1 mM in DMSO, were further diluted to 100 μM in Dulbecco's phosphate-buffered saline. The compounds were stored at -20°C and thawed on the day of experiments.

All animal procedures were conducted in accordance with protocols approved by the Illinois Institutional Animal Care and Use Committee at the University of Illinois at Urbana-Champaign and in compliance with the ARRIVE guidelines [26]. For the experiments with frozen brain slices, three 10 to 11-months-old 5xFAD (Jackson Laboratories) mice and one wildtype (WT, C57BL/6)

control were sacrificed by cardiac perfusion with saline. The whole brain was extracted postmortem and frozen at -80°C . The samples were cut to 300 μm thick slices using a vibratome and placed in $\times 1$ PBS on the imaging stage. After the acquisition of label-free images, the compounds were topically added using a pipette and mixed twice by swishing the fluid up and down twice immediately after addition.

For in vivo binding of compounds in the brain, a 10-months-old 5xFAD (Jackson Laboratories) mouse and a wildtype mouse (WT, C57BL/6) were intravenously injected with 1 mg/kg LS-4 per body weight for 10 days every day at a concentration of 1 mM in PBS (pH 7.4) with 1% DMSO. Each mouse was sacrificed by cardiac perfusion with saline, the brain was resected and 300 μm thick slices were produced using a vibratome. All FLIM images were acquired from the hippocampal region.

3 | RESULTS AND DISCUSSION

3.1 | Tracking the binding of topically applied LS-4 and ZY-12-OMe on frozen brain slices using SLAM microscopy

Both LS-4 and ZY-12-OMe were previously shown to have very broad emission spectra from 440 to 600 nm [9–11]. In SLAM microscopy, this is expected to create fluorescent signals in the blue, green and yellow channels (corresponding to 3PEF, SHG and 2PEF channels for label-free imaging, respectively), which is observed when imaging the compounds in PBS. First, across all channels, ZY-12-OMe in PBS appears to be much brighter than LS-4 in PBS when excited at 1100 nm; both compounds had maximum fluorescence in the yellow channel (Figure 1A). Second, when topically added to brain slices, the compounds seem to accumulate around the edges after 1 h (Figure 1B–D). However, upon closer inspection, some regions indicated by the white arrows and circles appear to have increased fluorescence, suggesting that a part of the compound must have either had direct contact with these inner regions during topical application or permeated into the interior of the brain slices from the top or outer regions within the hour. These compounds were previously characterized with a blue-shift upon binding to $\text{A}\beta$ fibrils or oligomers [11]. Since the pure compound has maximum fluorescence in the 415 to 485 nm channel, we expect the fluorescence from the compounds bound to $\text{A}\beta$ to originate in the green/blue channels. The signal in the blue and green channels in the WT brain slice was negligible before the addition of the dye. Upon addition of ZY-12-OMe, there was significant increase in the intensities in the green and yellow

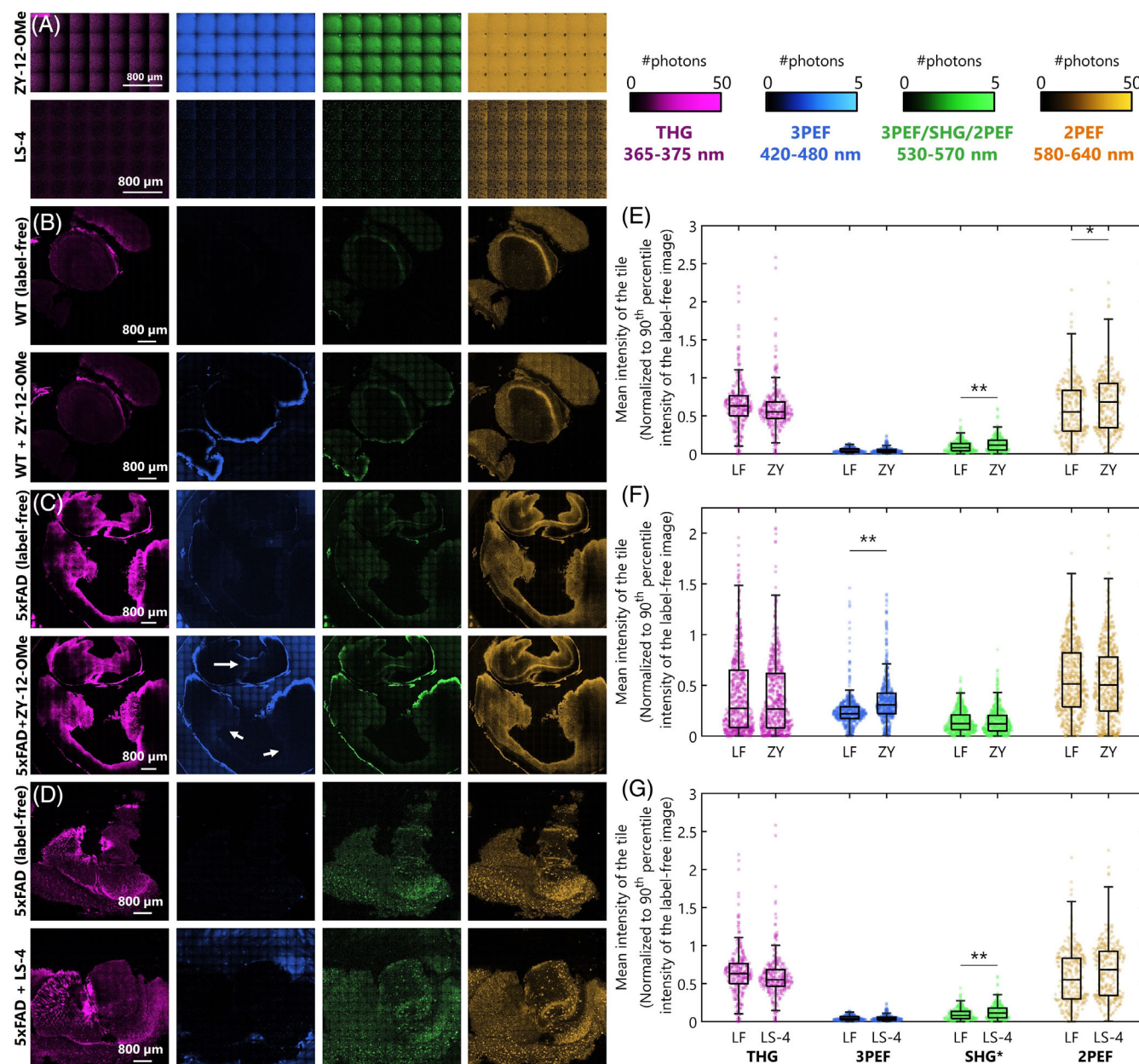


FIGURE 1 Tracking the binding of topically applied ZY-12-OMe and LS-4 on frozen brain slices from WT and 5xFAD mice using SLAM microscopy. SLAM images of (A) 30 μL of 100 μM of ZY-12-OMe and LS-4 in PBS. (B) Brain slice from WT mice before and 1 h after addition of 10 μL of 100 μM ZY-12-OMe. (C) Brain slice from 5xFAD mice before and 1 h after addition of 10 μL of 100 μM ZY-12-OMe. The white arrows show the sites where increased fluorescence is observed in the 3PEF channel. (D) Brain slice from 5xFAD mice before and 1 h after addition of 30 μL of 100 μM LS-4. (E-G) Comparison of normalized mean intensity of every 100×100 pixel tile within the brain slices (excluding the edges with abnormal diffusion/retention and empty spaces) in the four channels corresponding to B, C and D, respectively. LF: label-free (before addition of LS-4 and ZY-12-OMe); LS-4: 1 h after addition of 30 μL of 100 μM LS-4; ZY: 1 h after addition of 10 μL of 100 μM ZY-12-OMe; ** $p < .0005$; * $p < .005$; SHG*: SHG signal in the label-free image, a part of the emission spectra of the two compounds in labeled samples

channels (Figure 1B,E). In 5xFAD brain slices, this significant increase was instead observed in the blue channel corresponding to the expected spectral shift (Figure 1C, F). The sites with increased 3PEF fluorescence are in the hippocampus and cortex, where AD-related plaques are known to be abundant [1, 3, 4]. The increased

fluorescence from the binding of LS-4 to A β in 5xFAD mice was comparatively weaker, like the pure compounds. Nonetheless, there was a significant increase in the fluorescence intensity in the green channel (Figure 1D,G). These results correspond to the expected trends for these compounds. However, since their

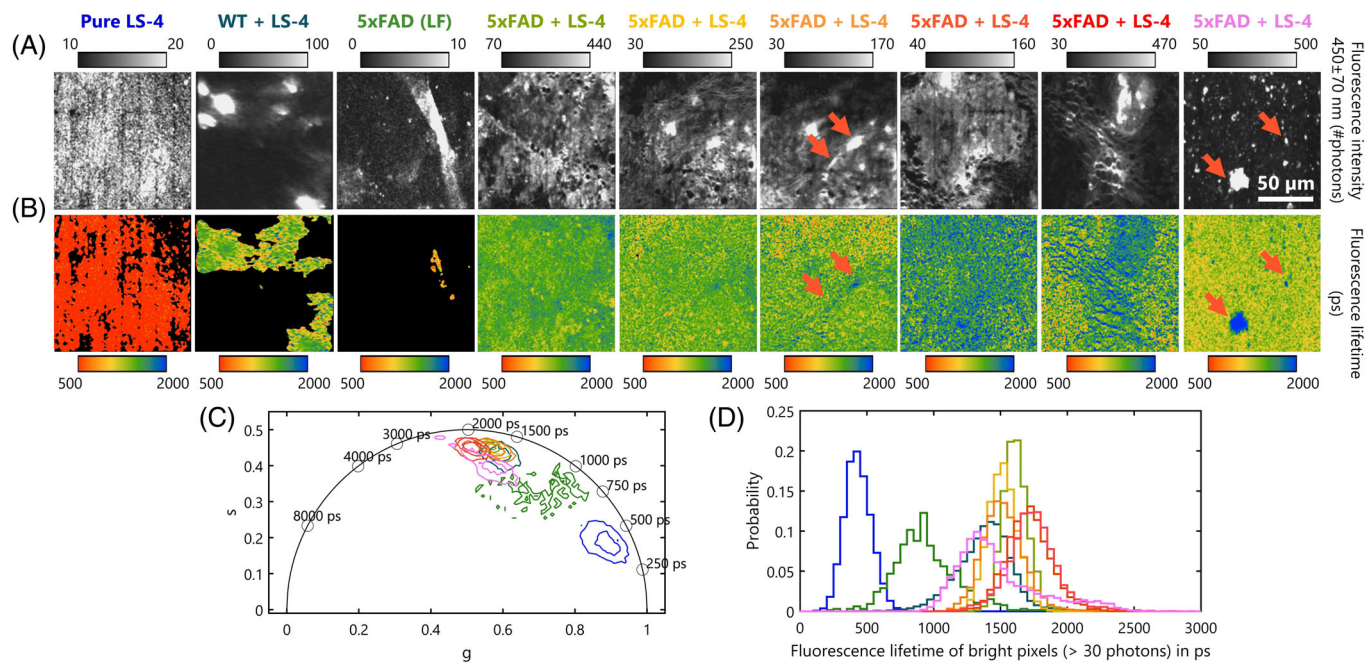


FIGURE 2 Tracking the binding of topically applied LS-4 on frozen brain sections in WT and 5xFAD mice. (A,B) Fluorescence intensity (A) and lifetime (B) of pure compound (blue), brain slice from WT with topically applied 50 μ L of 100 μ M LS-4 (dark green), brain slice from 5xFAD mice label-free (green) and two brain slices from 5xFAD with topically applied 50 μ L of 100 μ M LS-4 (olive to pink) collected using a 415 to 485 nm filter. (C,D) Phasor plots (C) and histogram of the fluorescence lifetime (D) for each frame following the same color scheme as A

fluorescence emission spectra are broad and overlapping for the different states of the compound, these samples were further characterized using FLIM in FOCALS which is expected to be more sensitive to the state of these compounds than intensity alone.

3.2 | Tracking the binding of topically applied LS-4 and ZY-12-OMe on frozen brain slices using fast FLIM

Next, we compared the multispectral analysis of fluorescence from pure LS-4 with FLIM in the 415 to 485 nm region (Figure 2). As observed using SLAM microscopy, 100 μ M of pure LS-4 was weakly fluorescent, emitting 10–20 photons for every 400 incident pulses; using fast FLIM the corresponding fluorescence lifetime was measured to be 300 to 500 ps. Similarly, the fluorescence of label-free 5xFAD brain was also weak (10 photons for 400 pulses) with a 2PEF lifetime of 750 to 1000 ps. The 2PEF values and the overall trend were calculated for the few pixels that were above the threshold to calculate accurate 2PEF lifetime values in the label-free image. The weak intrinsic fluorescence could be due to low NAD(P)H in the brain after freezing. Five minutes after the addition of 50 μ L of 100 μ M LS-4, the overall fluorescence intensities appear to be 10 to 50 \times higher than the

autofluorescence or fluorescence from LS-4 (Figure 1A). This suggests that the contribution of tissue autofluorescence or free LS-4 unassociated with the tissues or A β deposits can be neglected in our analysis after the addition of these compounds to the brain slices. The 2PEF lifetime of the brain slices after the addition of LS-4 was much higher than autofluorescence or the pure LS-4 (Figure 2B). Interestingly, the 2PEF lifetime of LS-4 even in control tissues from a WT mouse was much higher than pure LS-4, but lower than that of LS-4 in images from the 5xFAD mouse. Additionally, one of the images (pink frame) of LS-4 from 5xFAD mouse had similar 2PEF lifetime trends to that of the control slice in Figure 2D. Upon closer observation, this frame appears to be mostly devoid of any distinct tissue features, suggesting that this was a relatively empty region in the tissue (see FigureS2 for OCM images). However, some of these features have high 2PEF lifetimes (> 2000 ps). While none of the lifetime values. Compared with the distribution of lifetime values (Figure 2D), the distinction between the different populations (i.e., pure LS-4 (blue), autofluorescence (green), WT slice with LS-4 (dark green), empty regions in 5xFAD slices with LS-4 (pink and parts of yellow) and A β -rich regions of LS-4 [orange and red]) is more apparent in the phasor plots (Figure 2C). These results validate the turn-on or activation effect of LS-4 in tissue samples, the increased 2PEF

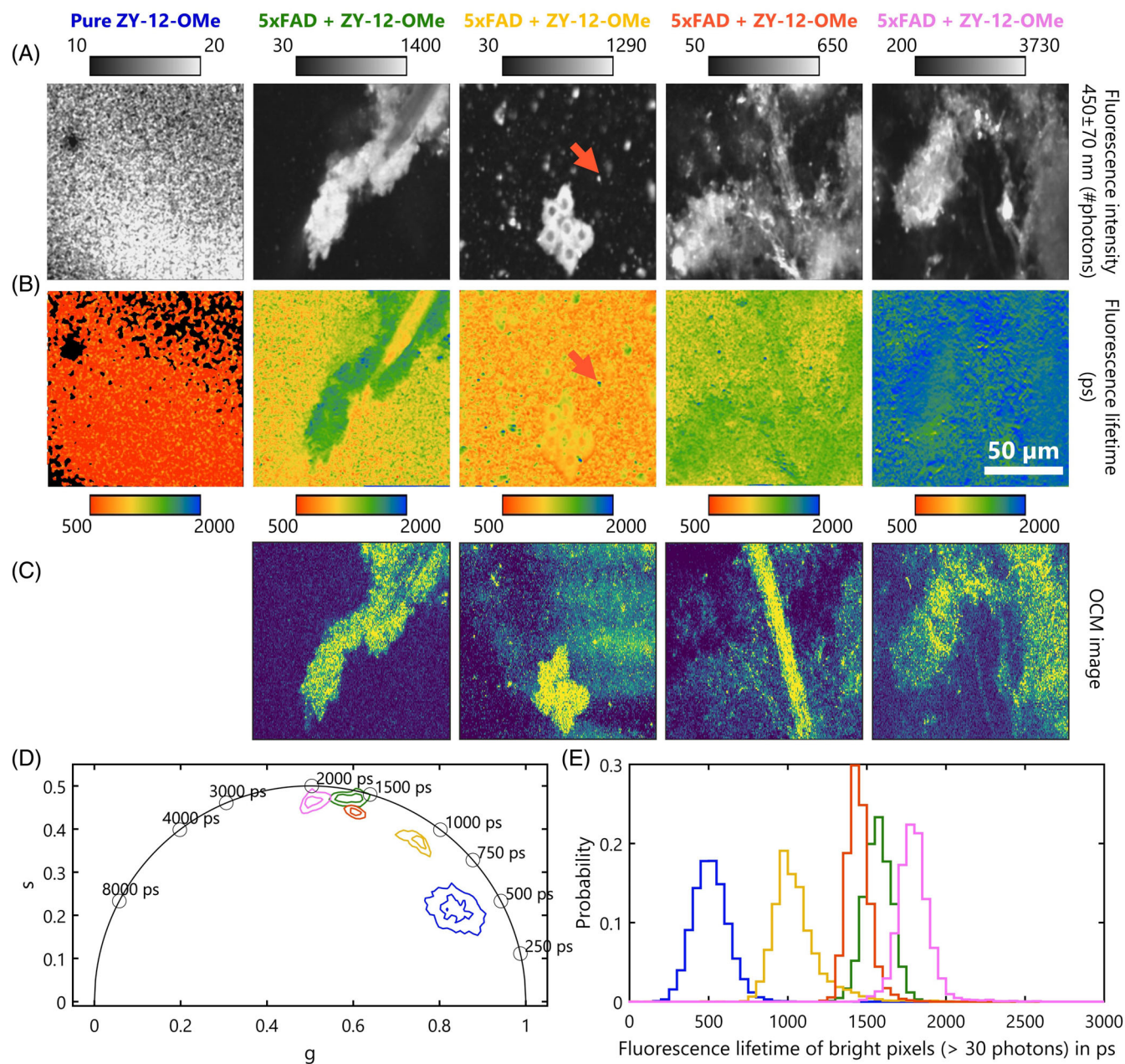


FIGURE 3 Tracking the binding of topically applied ZY-12-OMe on frozen brain sections from 5xFAD mice. (A,B) Fluorescence intensity (A) and lifetime (B) of the pure compound (blue) and two brain slices from 5xFAD with topically applied 50 μ L of 100 μ M ZY-12-OMe (green-orange: 5–7 min after, pink: 30 min after application) collected using a 415 to 485 nm filter. (C) OCM images corresponding to A and B. (D,E) Phasor plots (D) and histogram of the 2PEF lifetime (E) for each frame following the same color scheme as in A

lifetime of LS-4 immediately after addition to tissue samples, and how these 2PEF lifetime values are much higher when the compound is bound to A β plaque deposits. It is noteworthy that the pixels with high 2PEF lifetime also have high 2PEF intensity, suggesting that these compounds accumulate in certain regions that contain A β deposits and not in the empty spaces.

A similar trend is observed for ZY-12-OMe (Figure 3)—pure ZY-12-OMe has low 2PEF intensity (10–20 photons for 400 incident pulses) and lifetime (400–

600 ps). Compared with LS-4, the “turn-on” effect in fluorescence is much more prominent in 5xFAD brain slices (65–140 \times) within the first 5 min, and up to 370 \times after 30 min (Figure 3A). Like LS-4, the 2PEF lifetime of pure compounds is less than that of ZY-12-OMe in the tissue spaces, which is much lower than locations where it accumulates, indicating the presence of A β deposits (Figure 3B). The corresponding OCM images help identify locations with abnormal scattering that have high 2PEF lifetime (>2000 ps, indicated with the orange

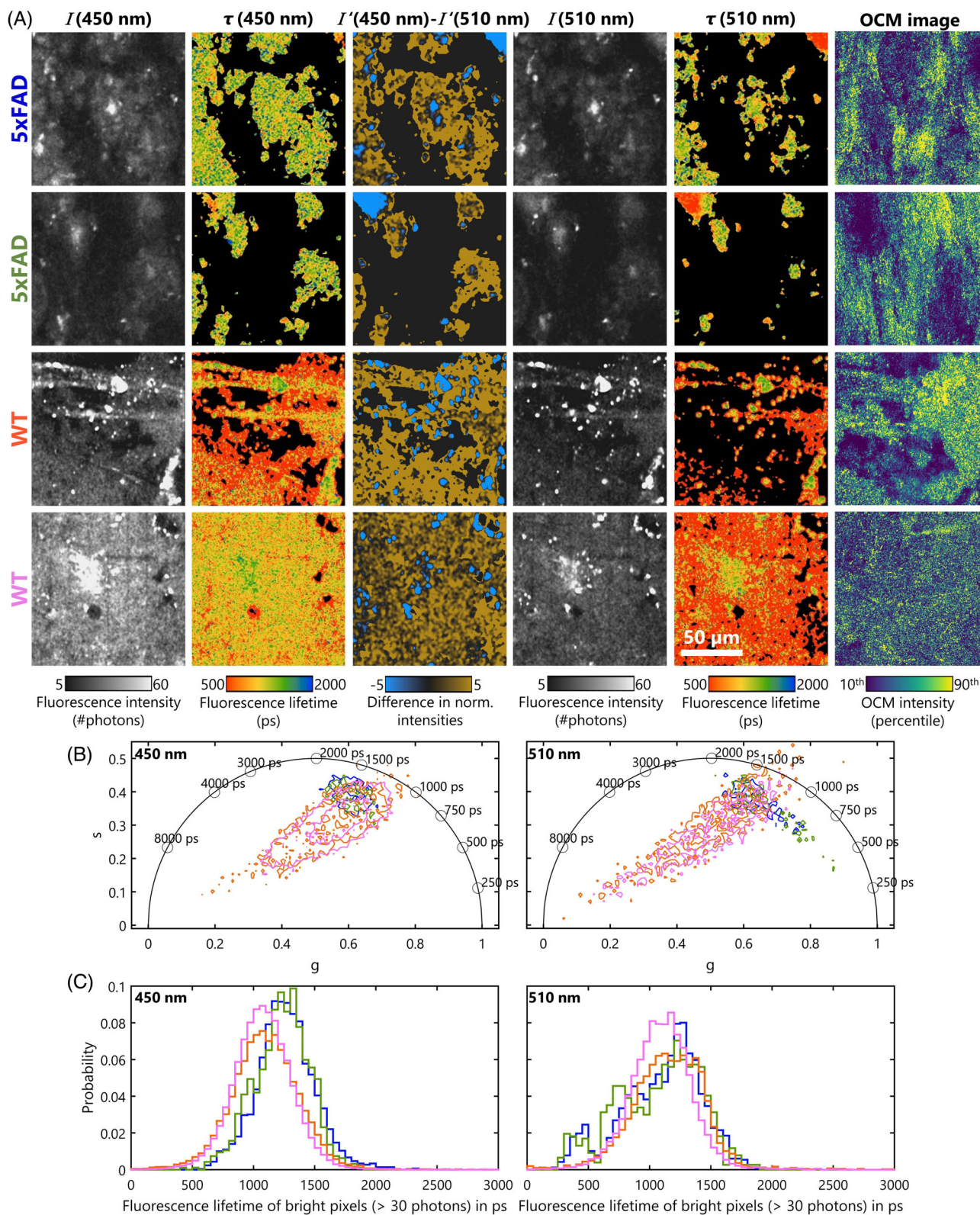


FIGURE 4 Tracking the binding of LS-4 after intravenous injections in WT and 5xFAD mice. (A) Fluorescence intensity and lifetime of brain slices from WT (orange and pink) and 5xFAD mice (blue and green) collected using two different filters: 415 to 485 nm (columns 1 and 2, respectively) and 468–552 nm (columns 4 and 5, respectively), the difference between the two fluorescence intensities normalized by their relative transmission and bandwidths (column 3), and the corresponding OCM images (column 6). (B,C) Phasor plots and histograms of the fluorescence lifetime for each frame acquired with the two different filters, following the same color scheme as in A for differentiating between WT and 5xFAD

arrows in Figure 3A,B), and regions that are mostly homogenous or empty which have higher 2PEF lifetime than pure ZY-12-OMe and lower than regions with A β deposits (Figure 3C). These distinctions are apparent in both the distributions of the fluorescence lifetime and the phasor plots (Figure 3D,E).

Despite the differences in the fluorescence efficiency of the compounds aside, the inferences regarding the relationship between the 2PEF characteristics and protein-binding made for LS-4 appear to be valid for ZY-12-OMe as well (Figure 2). FLIM appears much more sensitive to the binding of these compounds to different structures in the 5xFAD brain slices immediately after addition to tissues, even without washing off the unbound compounds.

3.3 | Tracking the binding of intravenously injected LS-4 on fresh 5xFAD (and WT) brain slices using fast FLIM

Having investigated the short-term binding of these compounds using topical application, we wanted track LS-4 in brain 10 days after daily intravenous injections. LS-4 was chosen over ZY-12-OMe for these experiments to show the potential of multimodal imaging with FLIM on the weaker of the two compounds. Additionally, to further explore the spectral shift that was previously observed (Figure 1), FLIM images were acquired with two different emission filters: 415 to 485 nm and 468 to 552 nm. Although there is considerable overlap between the two filters, the former is expected to the emission band for A β -bound compounds and the latter is expected to span the emission band of compounds not bound to A β . In fresh brain slices, the total fluorescence appears to be higher than that of pure compounds or autofluorescence from previously frozen brain tissue slices, even in WT mice (60 photons from 400 incident pulses), either due to residual dye or tissue autofluorescence. However, not all the scattering tissue structures seen on the OCM images have high enough fluorescence to estimate accurate 2PEF lifetime values. Since the circulatory system would inherently wash away any unbound compounds, unlike the case of topical application, this decreased fluorescence was expected.

In the third column of Figure 4A, the normalized fluorescence intensity in the two bands was compared. The gold areas indicate regions where the intensity in the 415–485 nm band ($I'(450\text{ nm})$) was higher than the intensity in the 468–552 nm band ($I'(510\text{ nm})$), the other way around in the blue regions. There appear to be minimal differences based on visual observation alone. However, upon closer inspection and

quantification, the percentages of the strongly golden areas, where $(I'(450\text{ nm}) - I'(510\text{ nm})) > 1$, are 35.6%, 18.2%, 54.9% and 62.8%, respectively, for each row, whereas the percentages of blue area, where $(I'(450\text{ nm}) - I'(510\text{ nm})) < 1$, are 64.4%, 81.8%, 45.1% and 37.2%, respectively, for each row. The slices from 5xFAD mice have a larger percentage of blue area compared with the WT mice. While this intensity metric was useful to observe an overall trend, the accumulation of these compounds in a few sites that we observed in FLIM is not discernable here.

Like the results in Figures 2 and 3, the 2PEF lifetime of 5xFAD slices appears to be higher compared with the WT slices, which is distinctly in the 415 to 485 nm band and less apparent in the 468 to 552 nm band (Figure 4C). On the phasor plots (Figure 4B), the WT slices have a much larger spread compared with the 5xFAD slices. Overall, these results indicate that the binding dynamics of the compounds are more apparent in FLIM than just intensity-based multiphoton microscopy. Additionally, FLIM of the 415 to 485 nm appears to characterize LS-4 binding better than the 468 to 552 nm band in the context of A β deposits, based on both the fluorescence intensities and lifetimes.

4 | DISCUSSION AND CONCLUSION

ZY-12-OMe was naturally brighter despite having a slightly lower binding affinity to A β aggregates compared with LS-4 [9–11]. Correspondingly, in both SLAM and FLIM images, ZY-12-OMe appeared to have higher fluorescence intensity in tissues and in the presence of A β deposits. A significant increase in fluorescence was observed in the 420 to 480 nm channels for the 5xFAD brain slices upon the addition of ZY-12-OMe; this increase in fluorescence was red-shifted in WT slices appearing in both the green and yellow channels (Figure 1E,F). The increased fluorescence in LS-4, although weaker, was also in the blue and green channels. Moreover, the increase in fluorescence could be observed distinctly in the regions corresponding to the cortex and hippocampus. However, the selectivity of both ZY-12-OMe and LS-4 towards A β oligomers compared with other forms of A β aggregates is low based on their dissociation constants [9–11]. Consequently, the fluorescence intensity in a single spectral band alone was insufficient to characterize their binding to the A β plaques in the AD brain accurately. The 2PEF lifetime could differentiate three distinct populations in ZY-12-OMe within the first 5 min, such that the 2PEF lifetime of free compounds was less than the 2PEF lifetime of the

compounds in normal tissue/background, which was less than the 2PEF lifetime of the compounds bound to A β deposits. These results validate the previous characterization of the compounds based on fluorescence spectroscopy and simulations of protein interactions [9–11]. The observed different fluorescence lifetime values for the two compounds could be due to the slightly different modes of interaction with the A β aggregates that may lead to different extents of steric constraints for the excited state geometry, which will have a direct effect on their fluorescent lifetimes. Another source of variability is that the distribution of A β aggregates differs even within sub-regions in the brain and between different animals.

Apart from imaging the fluorescent tags, SLAM and FOCALS microscopy were also able to image several autofluorophores, harmonophores and other features in the brain slices. Particularly in SLAM, significant signals were observed in both the THG and 2PEF channels, corresponding to optical interfaces with mismatched refractive indices and to FAD, respectively. In these channels, the texture of the brain slice from 5xFAD mouse appears to be more heterogeneous with distinct granular structures compared with the brain slice from the WT mouse. For fluorescence characterization of the compounds, the THG channel was outside the emission spectra. However, THG is the only channel that relies solely on structural components. Therefore, the local heterogeneity was quantified as the ratio between the standard deviation and the mean intensity of 50×50 pixel tiles before the addition of the dye (Figure S3). The 5xFAD brain slices had significantly higher heterogeneity compared with the WT slice. This heterogeneity could be due to large protein deposits that have abnormally high local refractive indices or structural consequences of neuronal degradation from AD. Similarly, heterogenous structures were observed using X-ray phase-contrast microscopy [27] and optical coherence tomography in 5xFAD mice brains [28]. Furthermore, FOCALS microscopy showed that there were label-free features that could be obtained simultaneously with fluorescence characterization, such as the structures observed in the OCM images. Therefore, multimodal quantitative multiphoton microscopy was not only utilized to track the dynamics of exogenous markers of AD, but also discover possible label-free biomarkers of AD. Using the two modalities also enabled looking at the distribution of these compounds at two different spatio-temporal scales.

This study was driven by the motivation that multiphoton microscopy was more appropriate than confocal microscopy for thick tissue imaging due to its ability to image deeper, provide intrinsic axial sectioning, and have easier scalability to whole tissue or in vivo imaging in the future. We demonstrated that SLAM and FLIM not only extracted binary differences between 5xFAD and

WT slices based on the fluorescence of the tested compounds, like shown previously using confocal and widefield fluorescence imaging but also helped analyze the binding of the tags themselves with micron-scale resolution immediately after application to tissues based on their spectral responses and fluorescence lifetimes. SLAM and FOCALS microscopy were effectively utilized to investigate the fast-acting binding and theragnostic potential of these molecules. Furthermore, potentially novel label-free biomarkers based on the local heterogeneity were observed with our techniques that could complement the information from these fluorescent tags. In the future, we plan to extend these studies to observe the interaction of these compounds intravitaly with different types of A β deposits and at different stages of AD to study the mechanism behind their theragnostic effect.

AUTHOR CONTRIBUTIONS

Conceptualization: Rishyashring R. Iyer, Carlos A. Renteria, Liang Sun, Zhengxin Yu, Yiran Huang, Marina Marjanovic, Liviu M. Mirica and Stephen A. Boppart; Instrumentation: Rishyashring R. Iyer, Carlos A. Renteria, Lingxiao Yang, Janet E. Sorrells and Jaena Park, Investigation: Rishyashring R. Iyer, Carlos A. Renteria, Lingxiao Yang, Janet E. Sorrells and Jaena Park, Formal analysis, visualization and investigation: Rishyashring R. Iyer; Biological and chemical resources: Liang Sun, Zhengxin Yu, Yiran Huang and Liviu M. Mirica; Methodology: Rishyashring R. Iyer, Carlos A. Renteria and Stephen A. Boppart; Writing: Rishyashring R. Iyer and Stephen A. Boppart with input from all authors; Supervision and funding acquisition: Liviu M. Mirica and Stephen A. Boppart.

ACKNOWLEDGMENTS

The authors would like to thank Eric Chaney and Darold R. Spillman Jr. for their assistance in coordinating and executing this study. Additional information can be found at: <https://biophotonics.illinois.edu>.

FUNDING INFORMATION

This research was supported in part by grants from the National Institutes of Health (R01-CA241618, R01-GM114588) and the Air Force Office of Scientific Research (FA9550-17-1-0387). Carlos A. Renteria was supported by an NIH/NIEHS Fellowship Training Program in Endocrine, Developmental and Reproductive Toxicology (T32-ES007326). Rishyashring R. Iyer was supported partly by the Mavis Future Faculty Fellows program from the Grainger College of Engineering at the University of Illinois at Urbana-Champaign and partly supported by the Tissue Microenvironment Training Program funded by National Institute of Biomedical Imaging

and Bioengineering of the National Institutes of Health (T32-EB019944). Janet E. Sorrells was supported by a National Science Foundation Graduate Research Fellowship (DGE-1746047).

CONFLICT OF INTEREST

The method and apparatus reported here for processing FLIM images using SPEED has been disclosed as intellectual property by Janet E. Sorrells, Rishyashring R. Iyer, and Stephen A. Boppart to the Office of Technology Management at the University of Illinois at Urbana-Champaign. The authors declare no other conflicts of interests.

DATA AVAILABILITY STATEMENT

The data that support the findings of this study are available from the corresponding author upon reasonable request and through collaborative investigations.

ORCID

Rishyashring R. Iyer  <https://orcid.org/0000-0001-9126-9491>

Carlos A. Renteria  <https://orcid.org/0000-0002-3596-5799>

Lingxiao Yang  <https://orcid.org/0000-0002-9678-860X>

Janet E. Sorrells  <https://orcid.org/0000-0003-0071-8509>

Stephen A. Boppart  <https://orcid.org/0000-0002-9386-5630>

REFERENCES

- [1] J. Weller and A. Budson, *F1000Res* (2018), 7. <https://doi.org/10.12688/f1000research.14506.1>
- [2] Alzheimer's Association, *Alzheimers Dement.* **2018**, 14, 367.
- [3] L. Mucke, D. J. Selkoe, *Cold Spring Harb. Perspect. Med.* **2012**, 2, a006338.
- [4] H. Oakley, S. L. Cole, S. Logan, E. Maus, P. Shao, J. Craft, A. Guillozet-Bongaarts, M. Ohno, J. Disterhoft, L. van Eldik, R. Berry, R. Vassar, *J. Neurosci.* **2006**, 26, 10129.
- [5] H. Amijee, D. I. C. Scopes, *J Alzheimers Dis* **2009**, 17, 33.
- [6] S. Brahmachari, A. Paul, D. Segal, E. Gazit, *Future Med. Chem.* **2017**, 9, 797.
- [7] F. Re, C. Airoidi, C. Zona, M. Masserini, B. L. Ferla, N. Quattrocchi, F. Nicotra, *Curr Med Chem* **2010**, 17, 2990.
- [8] A. J. Doig, P. Derreumaux, *Curr. Opin. Struct. Biol.* **2015**, 30, 50.
- [9] L. Sun, H.-J. Cho, S. Sen, A. S. Arango, T. T. Huynh, Y. Huang, N. Bandara, B. E. Rogers, E. Tajkhorshid, L. M. Mirica, *J. Am. Chem. Soc.* **2021**, 143, 10462.
- [10] L. Sun, A. K. Sharma, B.-H. Han, L. M. Mirica, *ACS Chem. Neurosci* **2020**, 11, 2741.
- [11] Z. Yu, W. Guo, H.-J. Cho, S. Patel, L. M. Mirica, *Chem Rxiv* **2021**. <https://doi.org/10.26434/chemrxiv.14191856.v1>.
- [12] H. W. Ejaz, W. Wang, M. Lang, *Int. J. Mol. Sci.* **2020**, 21, E7660.

- [13] C. Gotzmann, F. Braun, M. D. Bartholomä, *RSC Adv.* **2016**, 6, 119.
- [14] H. F. Kung, S. R. Choi, W. Qu, W. Zhang, D. Skovronsky, *J. Med. Chem.* **2010**, 53, 933.
- [15] A. Boländer, D. Kieser, C. Scholz, R. Heyny-von Haußen, G. Mall, V. Goetschy, C. Czech, B. Schmidt, *Neurodegener Dis* **2014**, 13, 209.
- [16] M. Necula, R. Kayed, S. Milton, C. G. Glabe, *J. Biol. Chem.* **2007**, 282, 10311.
- [17] J. Dong, R. Revilla-Sanchez, S. Moss, P. G. Haydon, *Neuropharmacology* **2010**, 59, 268.
- [18] Y. W. Jun, S. W. Cho, J. Jung, Y. Huh, Y. Kim, D. Kim, K. H. Ahn, *ACS Cent. Sci* **2019**, 5, 209.
- [19] H. Tu, Y. Liu, D. Turchinovich, M. Marjanovic, J. K. Lyngsø, J. Lægsgaard, E. J. Chaney, Y. Zhao, S. You, W. L. Wilson, B. Xu, M. Dantus, S. A. Boppart, *Nat Photon* **2016**, 10, 534.
- [20] S. You, Y. Sun, E. J. Chaney, Y. Zhao, J. Chen, S. A. Boppart, H. Tu, *Biomed Opt. Express* **2018**, 9, 5240.
- [21] S. You, H. Tu, E. J. Chaney, Y. Sun, Y. Zhao, A. J. Bower, Y.-Z. Liu, M. Marjanovic, S. Sinha, Y. Pu, S. A. Boppart, *Nat. Commun.* **2018**, 9, 2125.
- [22] R. R. Iyer, J. E. Sorrells, L. Yang, E. J. Chaney, D. R. Spillman, B. E. Tibble, C. A. Renteria, H. Tu, M. Žurauskas, M. Marjanovic, S. A. Boppart, *Sci. Rep.* **2022**, 12, 3438.
- [23] S. You, Y. Sun, E. J. Chaney, Y. Zhao, J. Chen, S. A. Boppart, H. Tu, *Biomed Opt. Express* **2018**, 9, 5253.
- [24] J. E. Sorrells, R. R. Iyer, L. Yang, E. J. Chaney, M. Marjanovic, H. Tu, S. A. Boppart, *Opt. Express* **2021**, 29, 37759.
- [25] J. E. Sorrells, R. R. Iyer, L. Yang, A. J. Bower, D. R. Spillman, E. J. Chaney, H. Tu, S. A. Boppart, *Biomed Opt. Express* **2021**, 12, 4003.
- [26] N. Percie du Sert, V. Hurst, A. Ahluwalia, S. Alam, M. T. Avey, M. Baker, W. J. Browne, A. Clark, I. C. Cuthill, U. Dirnagl, M. Emerson, P. Garner, S. T. Holgate, D. W. Howells, N. A. Karp, S. E. Lazic, K. Lidster, C. J. MacCallum, M. Macleod, E. J. Pearl, O. H. Petersen, F. Rawle, P. Reynolds, K. Rooney, E. S. Sena, S. D. Silberberg, T. Steckler, H. Würbel, *PLoS Biol.* **2020**, 18, e3000410.
- [27] B. R. Pinzer, M. Cacquevel, P. Modregger, S. A. McDonald, J. C. Bensadoun, T. Thuering, P. Aebischer, M. Stampanoni, *Neuro Image* **2012**, 61, 1336.
- [28] J. Zhu, H. R. Freitas, I. Maezawa, L. Jin, V. J. Srinivasan, *Light Sci Appl* **2021**, 10, 145.

SUPPORTING INFORMATION

Additional supporting information can be found online in the Supporting Information section at the end of this article.

How to cite this article: R. R. Iyer, C. A. Renteria, L. Yang, J. E. Sorrells, J. Park, L. Sun, Z. Yu, Y. Huang, M. Marjanovic, L. M. Mirica, S. A. Boppart, *J. Biophotonics* **2022**, 15(9), e202200105. <https://doi.org/10.1002/jbio.202200105>